19th Brazilian Congress of Thermal Sciences and Engineering
November 06th-10th, 2022, Bento Gonçalves - RS - Brazil

ENC-2022- 0471
OPTIMIZATION OF THERMAL ABLATION FOR FUNCTIONAL RE-ENTRY ARRHYTHMIAS

Eber Dantas
Helcio R.B. Orlande
Department of Mechanical Engineering, Politécnica/COPPE, Federal University of Rio de Janeiro
eberdantas@mecanica.coppe.ufrj.br
helcio@mecanica.coppe.ufrj.br

George S. Dulikravich
Department of Mechanical and Materials Engineering, Florida International University
dulikrav@fiu.edu

Abstract. *Cardiac arrhythmias are a global health problem associated with various heart conditions and responsible for a significant number of deaths related to sudden cardiac arrest. Thermal ablation is the most common treatment in correcting anomalous heartbeats. However, there are still several limitations to the procedure and varying degrees of success are noticed depending on the type of arrhythmia; for example, in some cases multiple repeated procedures are usually required to achieve stabilization. For the case of rotor-driven functional re-entry arrhythmias, natural heterogeneities of the cardiac tissue cause complex phenomena, as generation of spiral/scroll waves for the electrophysiological signal and dangerous wave break dynamics, which may cause sustained fibrillation. This works analyzes the optimization of thermal ablation procedures for functional re-entry arrhythmias, considering the optimal selection for the position of a radiofrequency electrode. An idealized two-dimensional rectangular region of the cardiac muscle is examined for various positions and sizes of a rectangular heterogeneous tissue that induces re-entry. A radiofrequency electrode is considered as being introduced in the endocardium side, heating the tissue. A two-dimensional bioheat transfer problem was solved with an energy generation term that results from the radiofrequency problem. Thermal damage was given by the Arrhenius' model and was used to modify electrophysiology parameters in a spatially continuous fashion. Besides a region of acute lesion, this introduces zones of intermediary damage levels. Then, the Fenton-Karma model was used in this work to simulate the electrophysiology dynamics. The optimization problem is structured according to the electrode position for thermal ablation, aiming at minimizing an objective function that reflects the transmission of electrophysiological signals in undesired directions. A Differential Evolution algorithm was used to solve the optimization problem in different conditions of functional re-entry. The results reveal interesting features for the choice of objective function, especially in determining the quality of solution and how the interplay between the chosen models affect the methodology.*

Keywords: *Rotor-driven Arrhythmia, Functional Re-entry, Thermal Ablation, Differential Evolution Optimization, Cardiac Muscle Electrophysiology*

1. INTRODUCTION

Cardiac arrhythmias are an ongoing global health problem. In the past years, sudden cardiac death has been a leading cause of mortality in the industrialized world, with a significant proportion caused by ventricular arrhythmias, especially in patients with history of infarction (Arevalo et al., 2016). Cardiac ablation therapies are the main form of treatment in correcting these anomalous excitations of the heart (Lee et al., 2012), where a localized thermal destruction of tissue is performed to stop the arrhythmogenic process. While cardiac ablation therapies are constantly evolving, there are still serious limitations. For example, for the case of scar-related ventricular tachycardia there is no optimal strategy to identify the arrhythmogenic substrate (Anter et al., 2020). The comparative efficiency of catheter ablation is also highly dependent on the type of arrhythmias, and may in general require multiple procedures of ablation over time. For patients with persistent atrial fibrillation, the success rate of a single procedure of catheter ablation can be around 50% (Boyle et al., 2016), and in some instances as low as 20−30% (Lee et al., 2012). Long-term monitoring also reveals that a significant number of patients continue to suffer asymptomatic atrial fibrillation after ablation (Verma et al., 2013), and that success

without medications after one year is 40−60% when only one ablation procedure is performed for AF (reaching 70% for 3 or more procedures) (Cheema et al., 2006; Weerasooriya et al., 2011).

One reason for the difficulty of success of ablation procedures in some types of arrhythmias arise when there is no visible arrhythmogenic substrate, as is the case for functional re-entry arrhythmias (Antzelevitch and Burashnikov, 2011). In this arrhythmogenic process, natural heterogeneities in healthy cardiac tissue break the waves of action potential (AP, the electrophysiology signal that causes muscle contraction), generating rotors that induce spiral waves, thus propagating the signal in undesired directions, uncoordinated, with the risk of fibrillation. The heterogeneity of the tissue for this case is in respect to the restitution properties: the duration of an action potential for a certain region of the tissue is dependent on the diastolic interval (interval of time since the end of last AP), and this functional behavior can be different in adjacent regions. While clinical procedures targeting rotors during ablation have significant results (Naranyan et al., 2012), there is significant variability in success rate between studies using such strategies, depending on the monitoring time and professionals involved, which is indicative that an optimal ablation strategy has not been achieved (Parameswaran et al., 2018).

In this work, a numerical study is performed for the optimization of radiofrequency thermal ablation in a simplified 2D geometry that suffers from functional re-entry arrhythmia due to the presence of a rectangular inner region with different restitution properties than the rest. The choice of objective function is based on the idea of the expected direction of conduction for the action potential, which, if useful, may be potentially extended in future for more complicated scenarios by taking into account the anisotropy of the cardiac muscle fibers. The objective is to analyze if the choice of objective function is useful for the optimization problem in providing states without re-entry after performing ablation according to its minimization, and also to investigate its deficiencies that may be addressed in the future. The simulations were performed with a 2D Fenton-Karma electrophysiology model for the propagation of the action potential, using the bioheat equation for unipolar radiofrequency thermal ablation. Coupling between the models was considered with an Arrhenius' model for thermal damage that modified the electrophysiology domain in a spatially continuous fashion, introducing zones of sub-lethal damage. The control variable for the optimization was the electrode position, obtained with a differential evolution algorithm after minimization of the objective function. Four cases of re-entry setups were analyzed, varying the position and size of the heterogeneous inner region, and also considering two possible heating times for the ablation.

2. METHODOLOGY

Figure (1) summarizes the 2D domain of dimensions $L_x = 80$ mm by $L_y = 20$ mm for the three mathematical problems required for the simulations in this work. All its components are explained next in this section. This general setup was used previously by the authors in (Dantas et al., 2022) during exploration of various test cases, where all the values of the parameters and its references can be checked. The electrophysiology problem (Eqs. (1) to (7)) and the thermal problem (Eqs. (8)) were solved with a finite volume methodology, using the ADI method and Thomas algorithm, while the radiofrequency problem (Eq. (10)) was solved with a Gauss-Seidel iteration algorithm. In all the equations for this section, x and y represent the position according to Figure 1, in millimeters, t is time in milliseconds for the electrophysiology and time in seconds for the thermal ablation.

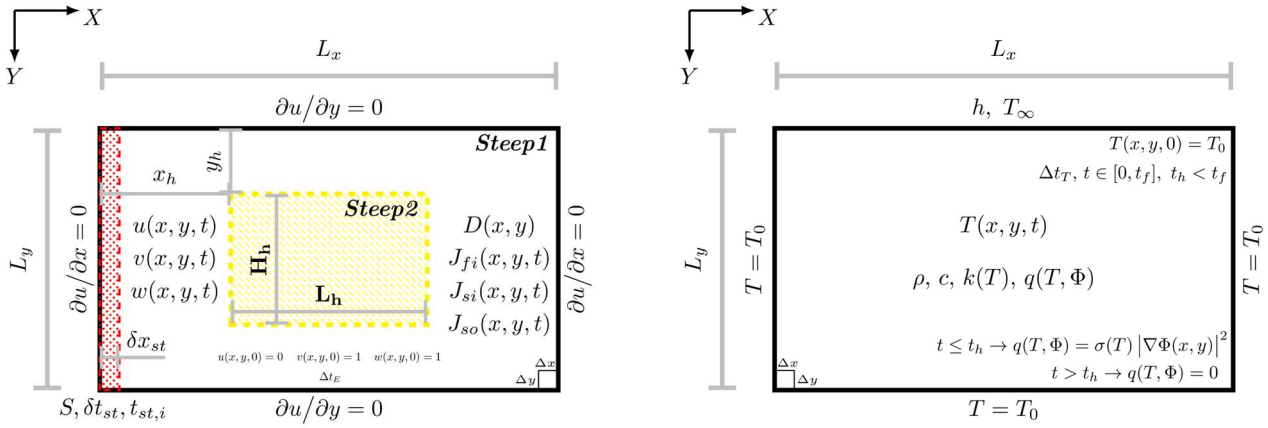

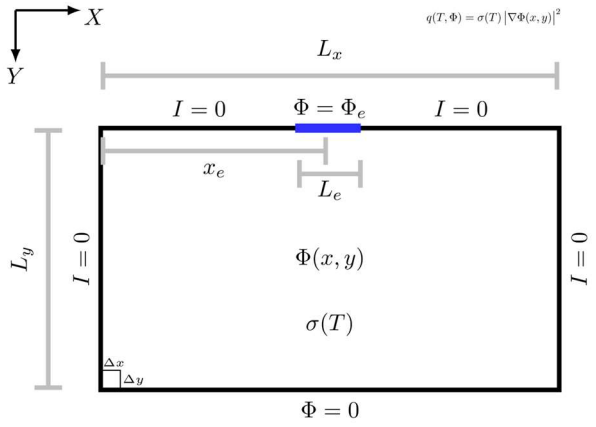

Figure 1. Diagrams for the domain of the three mathematical problems solved during the simulation. Top left: electrophysiology problem. Top right: thermal problem. Bottom: radiofrequency problem.

2.1 Electrophysiology

Propagation of action potential in a 2D domain was simulated with the phenomenological 3V-SIM model (Fenton and Karma, 1998; Fenton et al., 2002):

$$\frac{\partial u}{\partial t}(x,y,t) = \frac{\partial}{\partial x}\left(D(x,y)\frac{\partial u}{\partial x}\right) + \frac{\partial}{\partial y}\left(D(x,y)\frac{\partial u}{\partial y}\right) - J_{fi}(u,v) - J_{si}(u,w) - J_{so}(u)\,, \tag{1}$$

$$\frac{\partial v}{\partial t}(x,y,t) = -\frac{v}{\tau_v^+}H(u-u_c) + \frac{1-v}{\tau_v^-(u)}\left(1 - H(u-u_c)\right), \tag{2}$$

$$\frac{\partial w}{\partial t}(x,y,t) = -\frac{w}{\tau_w^+}H(u-u_c) + \frac{1-w}{\tau_w^-}\left(1 - H(u-u_c)\right), \tag{3}$$

$$\tau_v^-(u) = \tau_{v1}^- H(u-u_v) + \tau_{v2}^-\left(1 - H(u-u_v)\right), \tag{4}$$

$$J_{fi}(u,v) = -\frac{v}{\tau_d}(1-u)(u-u_c)H(u-u_c)\,, \tag{5}$$

$$J_{si}(u,w) = -\frac{w}{\tau_{si}}\left(\frac{1+\tan\left(c_{si}(u-u_{c,si})\right)}{2}\right), \tag{6}$$

$$J_{so}(u) = \frac{1}{\tau_r}H(u-u_c) + \frac{u}{\tau_0}\left(1 - H(u-u_c)\right). \tag{7}$$

Where u is the normalized electric potential, and the normalized ionic currents J are regulated by the dynamics of the gate variables v and w. The model considers three ionic currents: fast inward (J_{fi}), slow inward (J_{si}) and slow outward (J_{so}). The τ parameters are the timescales related to the stages of depolarization, repolarization, and refractoriness that occur during the action potential. The parameters u_c, u_c^{si}, and u_v are threshold potentials (normalized), c_{si} is a coefficient for the modulation of the hyperbolic tangent, and the Heaviside function is used in the equations above as H. The parameter D is the diffusivity coefficient. Most of the domain is assigned a set of parameters named *Steep1,* and a rectangular heterogeneous region uses *Steep2* parameters (Nash et al., 2006), with size L_H by H_h located at (x_h, y_h), as shown in Figure 1. All the boundaries are isolated. The initial conditions are $u = 0$, $v = 1$, and $w = 1$ for every point of the domain. Stimuli are introduced in the left boundary as source terms, causing signals to propagate towards the positive x direction (right): in Figure 1, S is the intensity of the stimuli, which are applied over the red region of length δx_{st} and height L_y, during an interval of δt_{st}, starting in the instants $t_{st,i}$ = 0, 200 and 320 ms.

The tissue is originally considered isotropic in relation to u (D would be constant for every point), but the notation $D(x,y)$ is introduced here in Eq. (1) because this parameter is spatially altered by thermal damage after ablation (see Eq. (13)).

2.2 Thermal ablation

The Penne's model for bioheat transfer was used for the thermal problem. Denoting temperature as T, and the heat source from the radiofrequency heating as q:

$$\rho c \frac{\partial T}{\partial t} = \frac{\partial}{\partial x}\left(k(T)\frac{\partial T}{\partial x}\right) + \frac{\partial}{\partial y}\left(k(T)\frac{\partial T}{\partial y}\right) + q(T,\Phi)\,, \tag{8}$$

where no blood perfusion nor metabolic heat generation were considered (Berjano, 2006; Zhang et al., 2016). The parameters of this model are the cardiac tissue density (ρ), specific heat (c) and thermal conductivity (k).

Temperature in the thermal problem during simulations was limited to 100°C, so no phase-change dynamics were involved. The top boundary was considered as responsible for convective cooling caused by blood (endocardium side), with convection heat transfer coefficient h. The remaining boundaries were set at 37°C, as well as the initial condition.

The heat source q comes from resistive heating in the tissue induced by the radiofrequency electrode,

$$q(T,\Phi) = \sigma(T)\,|\nabla\Phi(x,y)|^2\,, \tag{9}$$

where σ is the electrical conductivity and Φ is the electrical potential given by the radiofrequency problem:

$$\frac{\partial}{\partial x}\left(\sigma(T)\frac{\partial \Phi}{\partial x}\right) + \frac{\partial \Phi}{\partial y}\left(\sigma(T)\frac{\partial \Phi}{\partial y}\right) \;=\; 0\,, \tag{10}$$

The radiofrequency problem was set as an active electrode in the top boundary, with a diameter of $L_e = 2$ mm, with its center positioned at x_e (see Figure 1), maintaining a constant voltage of $\Phi_e = 25$ V (Huang and Miller, 2014) during a heating time t_h. The passive electrode (0 V) was taken as the bottom boundary, and the other boundaries were set as electrically insulated.

The parameters k in Eq. (8) and σ in Eq. (9)-(10) were considered as functions of T (in degree Celsius), both limited to below 100 °C (González-Suárez and Berjano, 2016; Trujillo and Berjano, 2013):

$$k(T) = 0.531 + 0.0012(T(x,y,t) - 37)\,, \tag{11}$$

$$\sigma(T) = 0.541\exp\big(0.015(T(x,y,t) - 37)\big)\,. \tag{12}$$

2.3 Thermal damage

A thermal damage coefficient Ω was computed with an Arrhenius' model, considering a spatially continuous modification of the domain, which alters the diffusivity coefficient and ionic currents of Eq. (1) according to the damage fraction originally associated to the definition of Ω (Pearce, 2010, Dantas et al., 2022):

$$\Omega\big(x,y,t_f\big) = \int_0^{t_f} A\,exp\left(-\frac{E_a}{R\,T(x,y,t')}\right)\mathrm{d}t'\,, \quad D_\Omega(x,y) = D(x,y)\cdot e^{-\Omega}\,, \quad J_\Omega(x,y,t) = J(x,y,t)\cdot e^{-\Omega}. \tag{13}$$

Where A is a frequency factor, E_a is the activation energy for the irreversible damage reaction, R is the universal gas constant, t_f is the final time, which includes heating and cooling simulated through the thermal problem, and the parameters D_Ω and J_Ω are used in Eq. (1) instead of D and J (sum of ionic currents) after ablation is used to modify the domain. Temperature T here is necessarily in kelvin units. This choice for the thermal damage model simulates the effects of a transition zone around the region of acute lesion (high Ω), where cardiac tissue is only partially destroyed.

2.4 Optimization of the thermal ablation

For this simplified setup, the expected healthy behavior would be for the action potential to propagate from left to right as a planar wave, meaning that it would be mostly uniform along the vertical direction. In the case that a wave breaks and initiates re-entry due to the heterogeneity of restitution properties, the spatial gradient of the electric potential will present significant (absolute) values for its vertical direction component (y direction, see Figure 1), because spiral formation occurs and now the signal travels along the vertical direction. Thus, the following objective function is considered for minimization:

$$G = \sum_{t=0}^{t_a}\sum_{x=0}^{x=L_x}\sum_{y=0}^{y=L_y}\left(\frac{\partial \mathrm{u}}{\partial y}(x,y,t)\right)^2, \tag{14}$$

where u is the electric potential in Eq. (1) and $t_a = 1000$ ms is a time of analysis for the optimization problem.

In this work, a differential evolution algorithm of type DE/1/rand/bin is used to select the position x_e of the radiofrequency electrode during ablation that minimizes the objective function G. The objective is to investigate if G correctly separates cases of re-entry and no re-entry and if its useful in an optimization problem.

The following are the parameters and conditions for the algorithm in all test cases presented below. Mutation factor 0.8, crossover probability 0.7, population size 8, control parameter x_e limited in the range [20,60] mm, initial population randomly sampled by a uniform distribution in the range. The stop criteria were: standard deviation of G in the population became less than 10^{-3}, or a maximum number of generations was reached (30).

While this version of G in Eq. (14) is directly connected to the hypotheses used for the simplified geometry of this work, the main motivation is that in the more realistic scenario the cardiac tissue is considerably anisotropic (Kotadia et al., 2020; Ho and Sánchez-Quintana, 2009; Valderrábano, 2007), with a preferential direction of conduction for the action potential along the muscle fibers. Thus, a geometric inspired objective function like G could be potentially useful by using the components of the gradient along the non-preferential directions for each point.

3. RESULTS

Four cases of re-entry setups were considered for optimization, changing the size and position of the inner region $Steep2$ that has different restitutions properties (see Figure 1): inner region with horizontal length $L_h = 20$ mm (E2) and 30 mm (E3), positioned $y_h = 0$ mm from the top border (E2A, E3A), or $y_h = 2$ mm (E2B, E3B). In all cases, the inner region had $H_h = 10$ mm of thickness and was horizontally centered. For each case, two possibilities of ablation were considered, with heating times $t_h = 20$ or 30 s, while the position x_e of the active radiofrequency electrode was varied according to the optimization of G in Eq. (14). Table 1 summarizes the results of the optimization for each case according to each heating time, along with the geometrical details of the inner region. The convergence of algorithm can be seen for all the results in Figure 2, where the value of G is displayed for the best candidate solution obtained at each generation.

Table 1. Result of the optimization procedure, for each case.

Case	L_h (mm)	x_h (mm)	y_h (mm)	t_h (s)	x_e(mm)
E2A	20	30	0	20	39.6
				30	29.0
E2B	20	30	2	20	38.4
				30	20.0
E3A	30	25	0	20	35.1
				30	25.5
E3B	30	25	2	20	34.5
				30	23.5

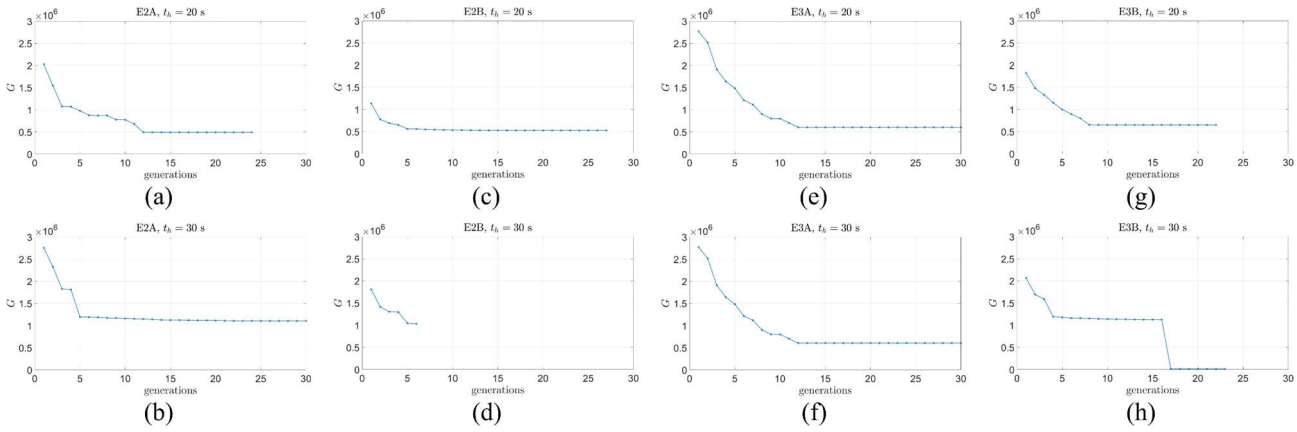

Figure 2. Convergence of the differential evolution algorithm for each result of Table 1. Value of objective function G in Eq. (14) for best candidate solution in each generation. (In 2.h, the attained minimum value of G is $1.1 \cdot 10^4$).

In all the remaining figures, the greyscale represents the normalized electric potential. Three signals are sent from the left at times 0 ms (S1), 200 ms (S2), 320 ms (S3), and the waves are the result of propagation of action potential (depolarization wavefront and repolarization "waveback"). The red level curves in the figures with ablation are isolines

of thermal damage that signify fractions of damage tissue: 18% (innermost), 63%, 86% and 98% (outermost). Figures are presented for representative cases of Table 1, while others with similar behavior are omitted for brevity.

For comparison, first consider Figure 3, where no ablation has been performed yet in case E2A, and thus re-entry occurs. The AP caused by S1 establishes the diastolic interval (interval of time) until S2 hits (3.a). Then, because the inner region has bigger values for its restitution properties, the wave brought by S2 takes longer to pass through there (longer AP duration), as can be seen in Figure 3.b. When S3 reaches, the region is still in a refractory state, which breaks the wave (3.c), forming a rotor (3.d), spiraling the signal (3.e), and causing re-entry (3.f), which makes the AP be sent in undesired directions (backwards, vertical, etc) and keeps forming spirals.

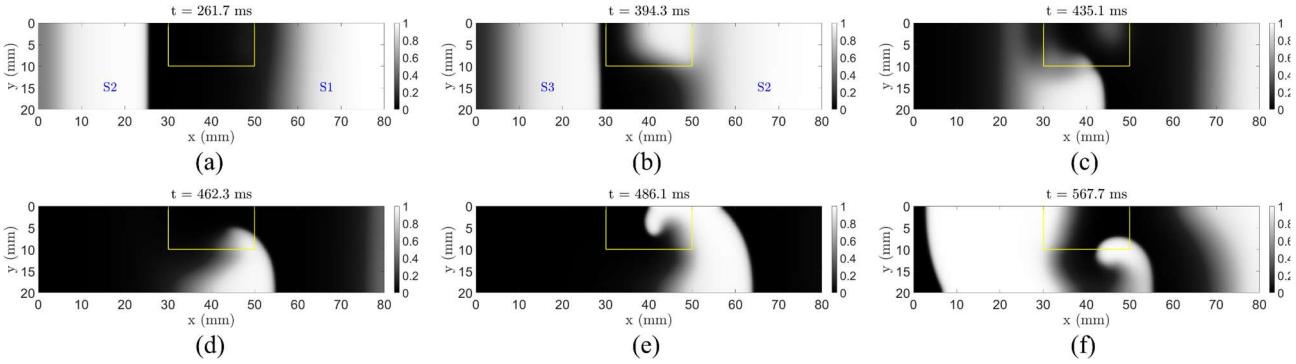

Figure 3. Case E2A ($L_h = 20$ mm, $y_h = 0$ mm), no ablation, re-entry occurs.

The optimization was successful in all test cases of Table 1 in finding a position x_e of the electrode that could stop re-entry from occurring. Figure 4 shows the solution $x_e = 39.6$ mm when using $t_h = 20$ s for case E2A (which had re-entry, as shown in Figure 2). Notice how the ablation is able to modify the dynamics to prevent the break of the S3 wave. The S3 wave went smoothly around the acute lesion (4.c) and reconnected to the top boundary, forming no rotor, and keeping the propagation of the action potential in the intended direction (from left to right).

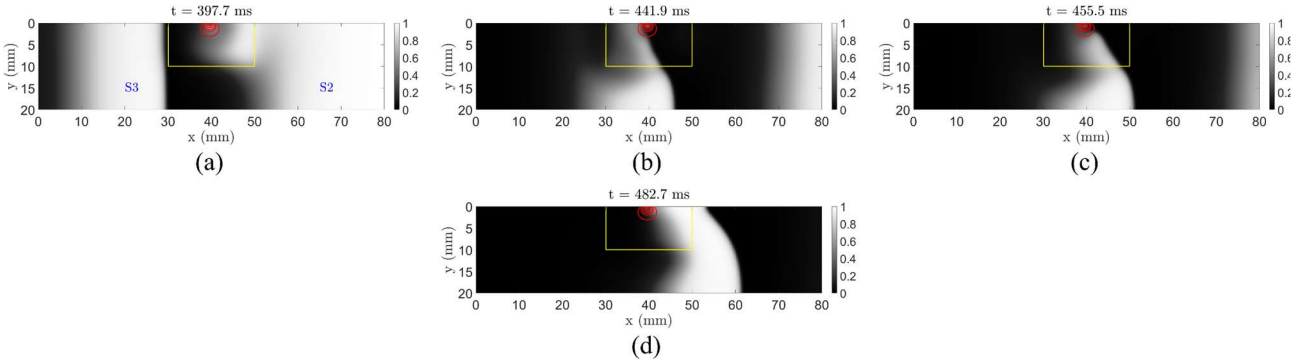

Figure 4. Optimization for case E2A ($L_h = 20$ mm, $y_h = 0$ mm) with $t_h = 20$ s ablation: $x_e = 39.6$ mm.

Similar behavior occurred for case E2B with $t_h = 20$ s (Figure 5), E3A with $t_h = 20$ s (Figure 6) and E3B with $t_h = 20$ s and 30 s. In all these situations, the S3 wave was capable of never breaking due to the modification brough by the ablation.

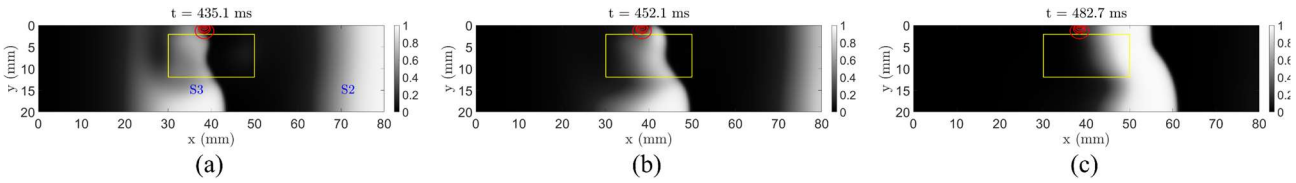

Figure 5. Optimization for case E2B ($L_h = 20$ mm, $y_h = 2$ mm) with $t_h = 20$ s ablation: $x_e = 38.4$ mm.

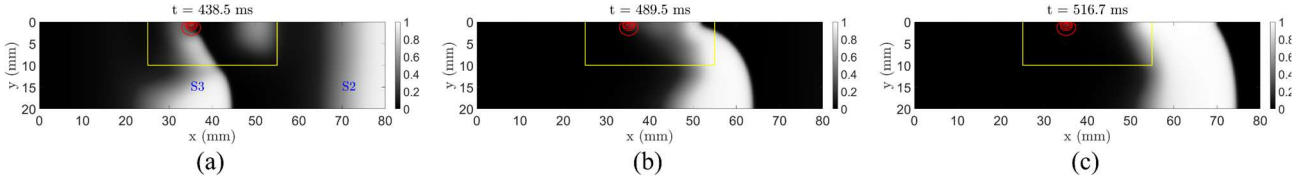

Figure 6. Optimization for case E3A ($L_h = 30$ mm, $y_h = 0$ mm) with $t_h = 20$ s ablation: $x_e = 35.1$ mm.

Although the optimization via the objective function G in Eq. (14) was able to find the ablation configurations that prevented re-entry for all setups, it is clear in Figure 7 that the S3 wave does break, even if no re-entry occurs. In Figure 7, case E2A after $t_h = 30$ s ablation at $x_e = 29.0$ mm presents a different behavior than previously, where the S3 wave is able to pass through the acute lesion without breaking but its top part is drained after travelling for a bit. This occurs due to the presence of the transition zone around the lesion, modeled by Eq. (13). Re-entry does not occur because the wavetip that was formed too close to the top boundary and got destroyed when it started to rotate the wave.

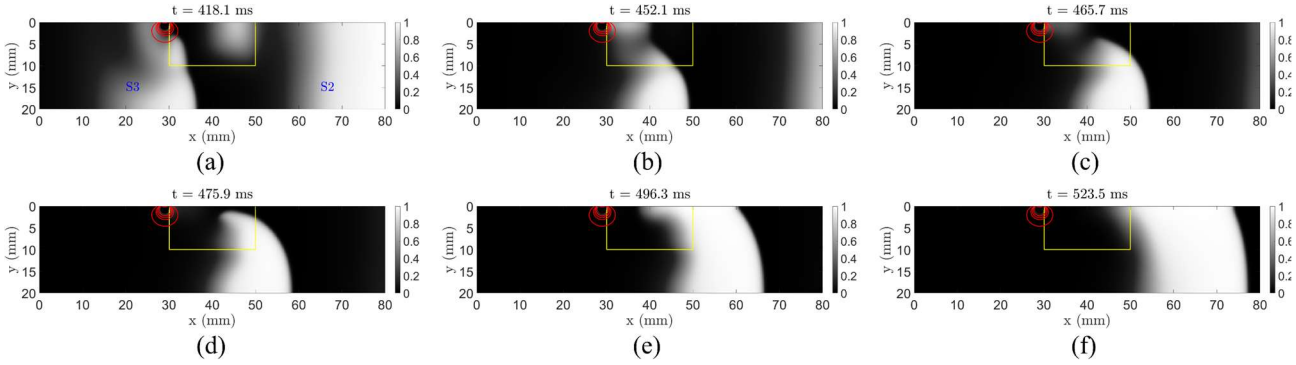

Figure 7. Optimization for case E2A ($L_h = 20$ mm, $y_h = 0$ mm) with $t_h = 30$ s ablation: $x_e = 29.0$ mm.

Similar behavior was noticed for case E2B with $t_h = 30$ s, and case E3A with $t_h = 30$ s (Figure 8).

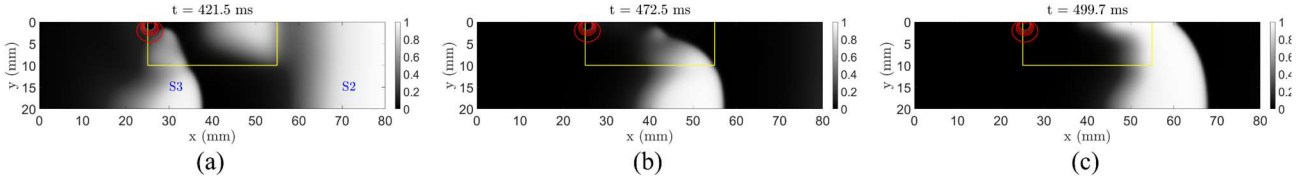

Figure 8. Optimization for case E3A ($L_h = 30$ mm, $y_h = 0$ mm) with $t_h = 30$ s ablation: $x_e = 25.5$ mm.

These results show that the choice of objective function G is indeed capable of providing no re-entry situations after ablation is performed according to its minimization. However, as shown in Figures 6 and 7, non-ideal solutions are also encountered, where re-entry is prevented but a wave break still happens (even though very briefly in Figure 8), which determines a more unstable solution that should be avoided, if possible, for more realistic applications. It would be beneficial that these non-ideal situations could be separated in the objective function from ideal solutions by significant values in G, so that in future analysis for more complicated problems (more control parameters, complex geometry, anisotropy, etc) the ideal solutions were selected when available.

4. CONCLUSION

Optimization of thermal ablation with one control variable for an idealized 2D setup of functional re-entry arrhythmia was performed for various cases, varying position and size of a heterogeneous rectangular inner region. The optimization considered the changing position of an active radiofrequency electrode, and an objective function was investigated to evaluate its usefulness. The function was based on a geometric argument related to the expected direction of propagation of action potential for the setup.

The objective function was capable of providing satisfactory solutions after minimization with a differential evolution algorithm. While its current iteration was tested for this simplified geometry that has a clear expected direction of propagation, the results are promising because in the more realistic scenario cardiac tissue presents a preferential direction of conduction of the electrophysiological signal (anisotropy). The authors are currently investigating the use of this

objective function with more control parameters for ablation in the idealized setup, intending to modify it for the general case with anisotropy so that this potential can be tested. Another observation during this investigation was that the current objective function does not provide a good enough distinction between solutions with "no re-entry and no break" (ideal) and "no re-entry but with a break" (non-ideal). A study for a penalization of the objective function aiming at correcting this limitation is also in the plan for the authors.

5. REFERENCES

Anter, E., Neuzil, P., Reddy, V.Y., et al, 2020. "Ablation of Reentry Vulnerable Zones Determined by Left Ventricular Activation From Multiple Directions: A Novel Approach for Ventricular Tachycardia Ablation". *Circ Arrhythm Electrophysiol*, Vol. 13, No. 6, pp. 23-45. DOI: 10.1161/CIRCEP.120.008625

Antzelevitch, C., and Burashnikov, A., 2011. "Overview of Basic Mechanisms of Cardiac Arrhythmia". *Card Electrophysiol Clin*, Vol. 3, No. 1, pp. 23-45. DOI: 10.1016/j.ccep.2010.10.012

Arevalo, H. J., Vadakkumpadan, F., Guallar, E., et al, 2016. "Arrhythmia risk stratification of patients after myocardial infarction using personalized heart models". *Nature Communications*, Vol. 7, No. 11437. DOI:10.1038/ncomms11437

Berjano, E.J., 2006. "Theoretical modeling for radiofrequency ablation: state-of-the-art and challenges for the future". *Biomed Eng Online*, Vol. 5, No. 24. DOI: 10.1186/1475-925X-5-24 2006

Boyle, P.M., Zahid, S., and Trayanova, N.A., 2016. "Towards personalized computational modelling of the fibrotic substrate for atrial arrhythmia". *Europace*, Vol. 18. No. 4, pp. 136-145. DOI: 10.1093/europace/euw358

Cheema, A., Vasamreddy, C.R., Dalal, D., et al, 2006. "Long-term single procedure efficacy of catheter ablation of atrial fibrillation". *J Interv Card Electrophysiol*, Vol. 15, No. 3, pp. 145-55. DOI: 10.1007/s10840-006-9005-9

Dantas, E., Orlande, H.R.B., and Dulikravich, G.S., 2022. "Thermal ablation effects on rotors that characterize functional re-entry cardiac arrhythmia". *Int J Numer Meth Biomed Engng*, e3614. DOI: 10.1002/cnm.3614

Fenton, F.H., and Karma, A., 1998. "Vortex dynamics in three-dimensional continuous myocardium with fiber rotation: Filament instability and fibrillation". *Chaos*, Vol. 8, No. 1, pp. 20-47. DOI: 10.1063/1.166311

Fenton, F.H., Cherry, E.M., Hastings, H.M., and Evans, S.J., 2002. "Multiple mechanisms of spiral wave breakup in a model of cardiac electrical activity". *Chaos*, Vol. 12, No. 3, pp. 852-892. DOI: 10.1063/1.1504242

González-Suárez, A. and Berjano, E., 2016. "Comparative Analysis of Different Methods of Modeling the Thermal Effect of Circulating Blood Flow During RF Cardiac Ablation". *IEEE Trans Biomed Eng*, Vol. 63, No. 2, pp. 250-9. DOI: 10.1109/TBME.2015.2451178

Ho, S.Y., and Sánchez-Quintana, D, 2009. "The importance of atrial structure and fibers". *Clin Anat*, Vol. 22, No. 1, pp. 52-63. DOI: 10.1002/ca.20634.

Huang, S. K. S., and Miller, J. M., 2014. *Catheter Ablation of Cardiac Arrhythmias*. Saunders, Philadelphia, 3rd edition. ISBN: 9780323529921

Kotadia, I., Whitaker, J., Roney, C., et al, 2020. "Anisotropic Cardiac Conduction". *Arrhythm Electrophysiol Rev*, Vol. 9, No. 4, pp. 202-210. DOI: 10.15420/aer.2020.04

Lee, G., Sanders, P., and Kalman, J.M., 2012. "Catheter ablation of atrial arrhythmias: state of the art". *The Lancet*, Vol. 380, No. 9852, pp. 1509-1519. DOI: 10.1016/S0140-6736(12)61463-9

Narayan, S.M., Krummen, D.E., Shivkumar, K., et al, 2012. "Treatment of Atrial Fibrillation by the Ablation of Localized Sources: CONFIRM (Conventional Ablation for Atrial Fibrillation With or Without Focal Impulse and Rotor Modulation) trial". *J Am Coll Cardiol*, Vol. 60, No. 7, pp. 628-636. DOI:10.1016/j.jacc.2012.05.022.

Nash, M.P., Bradley, C.P., Sutton, P.M., et al, 2006. "Whole heart action potential duration restitution properties in cardiac patients: a combined clinical and modelling study". *Experimental Physiology*, Vol. 91, No. 2, pp. 339-354. DOI: 10.1113/expphysiol.2005.031070

Parameswaran, R., Voskoboinik, A., Gorelik, A., et al, 2018; "Clinical impact of rotor ablation in atrial fibrillation: a systematic review". *Europace*, Vol. 20, No. 7, pp. 1099-1106. DOI: 10.1093/europace/eux370

Pearce, J. A., 2010. "Models for thermal damage in tissues: processes and applications". *Crit Rev Biomed Eng*, Vol. 38, No. 1, pp. 1-20. DOI: 10.1615/critrevbiomedeng.v38.i1.20

Trujillo, M., Berjano, E., 2013. "Review of the mathematical functions used to model the temperature dependence of electrical and thermal conductivities of biological tissue in radiofrequency ablation". *Int J Hyperthermia*, Vol. 29, No. 6, pp. 590-597. DOI: 10.3109/02656736.2013.807438

Valderrábano, M., 2007. "Influence of anisotropic conduction properties in the propagation of the cardiac action potential". *Prog Biophys Mol Biol*, Vol. 94, No. 1-2, pp. 144-68. DOI: 10.1016/j.pbiomolbio.2007.03.014

Verma, A., Champagne, J., Sapp, J., et al., 2013. "Discerning the incidence of symptomatic and asymptomatic episodes of atrial fibrillation before and after catheter ablation (DISCERN AF): a prospective, multicenter study". *JAMA Intern Med*, Vol. 173, No. 2, pp. 149-156. DOI:10.1001/jamainternmed.2013.1561.

Weerasooriya, R., Khairy, P., Litalien, J., et al, 2011. "Catheter Ablation for Atrial Fibrillation". *Journal of American College of Cardiology*, Vol. 57, No. 2, pp. 160-166. DOI:10.1016/j.jacc.2010.05.061

Zhang, B., Moser, M.A.J., Zhang, E. M., et al, 2016. "A review of radiofrequency ablation: Large target tissue necrosis and mathematical modelling". *Phys Med*, Vol. 32, No. 8, pp. 961-71. DOI: 10.1016/j.ejmp.2016.07.092

6. RESPONSIBILITY NOTICE

The authors are the only responsible for the printed material included in this paper.